Proceedings of the
Annual Stability Conference
Structural Stability Research Council
Orlando, Florida, April 12-15, 2016

Stability of perforated cold-formed steel beam-columns

Yared Shifferaw[1], Trevor Rabare[2]

Abstract

The objective of this research is to examine the stability of perforated cold-formed steel members subjected to combined axial and bending loads. Preliminary design formulations of the Direct Strength Method in non-perforated cold-formed steel beam-columns indicated that under combined actions, linear interaction assumption for predicting strength of cold-formed steel is conservative in comparison with direct-analysis prediction that considers stability and yielding of cold-formed steel beam-columns under the appropriate stress combinations. Perforated cold-formed steel members subjected to combined loading are commonly used in cold-formed steel framing industry and it is important to extend the beam-column stability examination to perforated members as well. Yielding and stability solutions under direct combined actions for perforated sections are established. These elastic buckling envelopes form the basis for formulating a preliminary Direct Strength Method and together with collapse analysis provide valuable analytical background in future experimental testing of perforated cold-formed steel beam-columns.

1. Introduction

Cold-formed steel (CFS) members with perforations are commonly used in low-rise residential and commercial applications, such as those used in rack manufacturing. Fig. 1 illustrates perforations in CFS members used to allow connections and utility cables to pass through.

a) 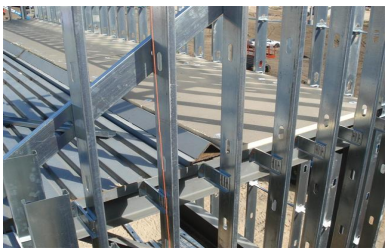 b) 

Figure 1: Cold-formed steel perforations in a) cold-formed metal framing b) deflection clip

[1]Asst. Prof., Civil, Architectural and Environmental Engineering, Drexel University, <yaredshi@drexel.edu>
[2]Graduate Student, Civil, Architectural and Environmental Engineering, Drexel University, <tr445@drexel.edu>

The Direct Strength Method (DSM) design for cold-formed steel extensively includes design formulations for pure compression and bending loads for non-perforated sections (Schafer (2008), AISI-S100 (2012)). The North American Specification of the American Iron and Steel Institute (AISI-S100 (2012)) in the past stated that, in determining the nominal strength for perforated sections, either axial or flexural, the same design formulations as non-perforated sections are used. This overlooked certain behavior observed in some sections where the failure occurs primarily at the hole resulting in reduction in capacity. Thus the same non-perforation design factors could not be applied in the design for sections with holes.

General design formulations for perforated sections with pure axial and bending loads are currently provided. These design specifications assume a linear interaction in the space between pure axial load and pure bending load. However, researchers have shown that strength predictions are beyond the linear assumption and vary non-linearly due to combined loading (Shifferaw and Schafer (2010), Shifferaw (2010).) Most cross sections used in the industry are perforated and are subjected to combined loads indicating the importance of extending combined loading design formulations for perforations since it is observed that the strength is not linear as assumed as shown in Fig. 2. Fig. 2 shows the definition of the P-M space (major axis bending is considered hence the resulting stresses lie on the first quadrant.) A generalized coordinate system is obtained by normalizing the axial and bending loads with axial and bending yield loads, P_y and M_y respectively. Points in the normalized P-M space are defined by angle θ and resultant diagonal length β as shown in Eq. 1 and Eq. 2:

$$\theta = tan^{-1}\left(\frac{M/M_y}{P/P_y}\right) \tag{1}$$

$$\beta = \sqrt{\left[\frac{P}{P_y}\right]^2 + \left[\frac{M}{M_y}\right]^2} \tag{2}$$

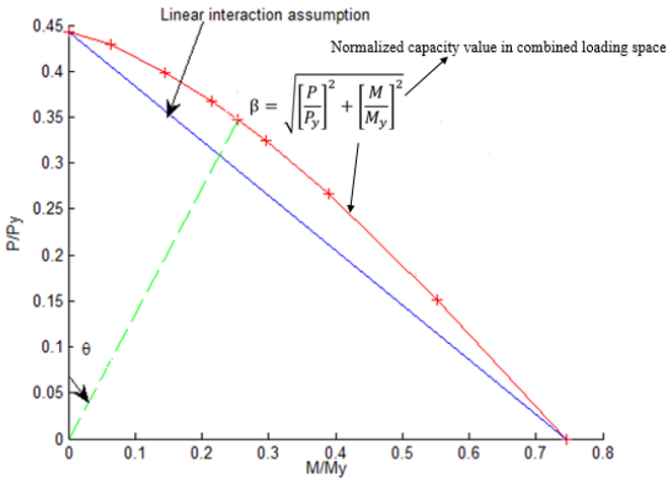

Figure 2: Normalized P-M space (Resultant diagonal length, β and azimuth angle θ)

2. Stability of perforated members under combined loading

2.1 Finite element computational modeling

A Steel Stud Manufacturers Association (SSMA) section 362S162-33 (3.625" web depth, flange width of 1.625” and 0.0346” thick) with a length of 48” is selected for convergence study. A slotted hole 4 in. long with a diameter of 1.5 in. is located at the center. Elastic modulus and Poisson ratio are set to 29500 ksi and 0.3 respectively. The section is loaded for θ =45°. The web is discretized into 4 elements transversely, while longitudinally the number of elements is varied. Boundary conditions are pinned at the ends and longitudinally pinned at mid-section to prevent warping.

Three thin shell element types in ABAQUS (2013) are considered: S4, S4R and S9R5. S4 and S4R are four node shell elements with linear shape functions while S9R5 is a nine-node shell element with a quadratic shape function. Fig. 3b shows the comparison of S4, S4R and S9R5 shell elements. S9R5 element does not diverge far from the converged eigenvalue of 3.4. This is because of its quadratic shape function, which enables it to capture a more accurate displacement within one element. In comparison, the S4 and S4R need a smaller aspect ratio in order to capture a similar behavior. This finding is in line with that of other researchers who have suggested computational modeling guides on cold-formed steel where S9R5 is recommended (Schafer et. al. (2010).)

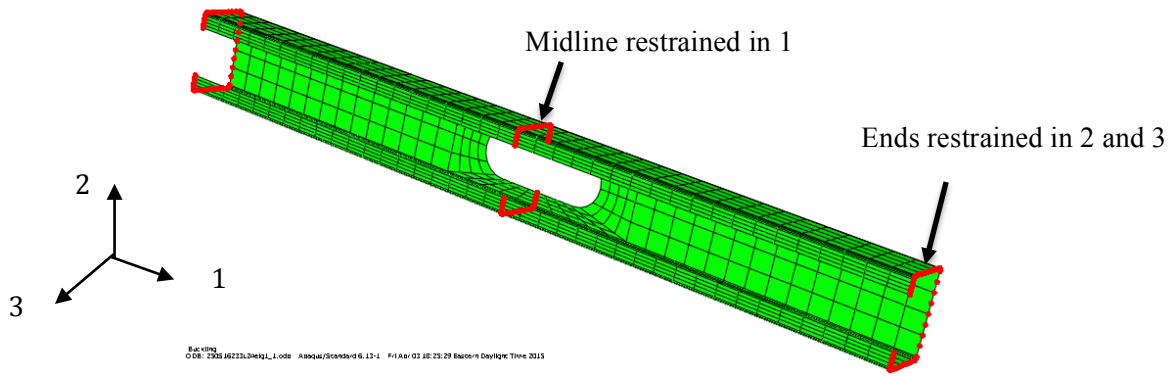

a)

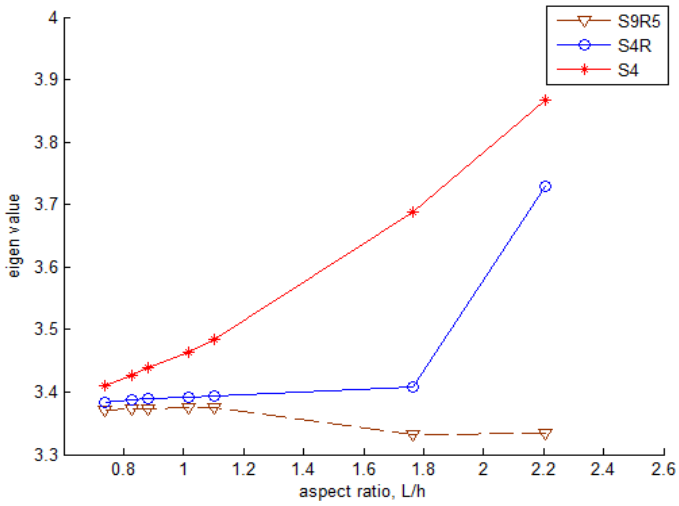

b)

Figure 3: Finite element modeling a) boundary conditions for a channel section b) sensitivity of ABAQUS shell elements by varying aspect ratio

2.2 Local stability

Local stability examination for SSMA sections (250S162-33 L24", 362S137-33 L48" and 600S162-33 L48") indicate two distinct local mode behaviors due to the presence of the perforation as shown in Fig. 4: a symmetric deformation around the hole (for lower θ) and unsymmetrical deformation around the hole (for higher θ). Comparisons of critical local buckling under combined loading for perforated and non-perforated members are shown in Fig. 5. The presence of the perforation induces increased reduction in the elastic critical buckling magnitude in comparison with the non-perforated member, particularly in the P-M space with higher flexural loading. For the shorter section 250S162-33, the perforation impact was not as significant in the P-M space with major axial contribution, in comparison with section 600S162-33.

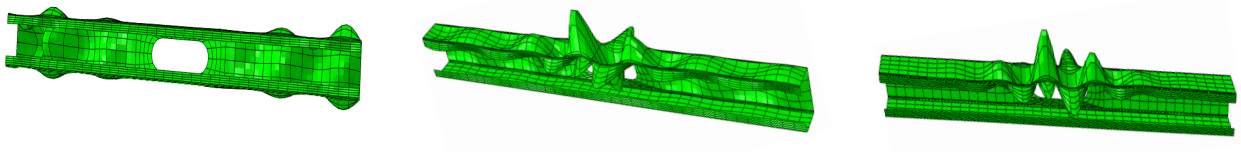

i. ii. iii.

a)

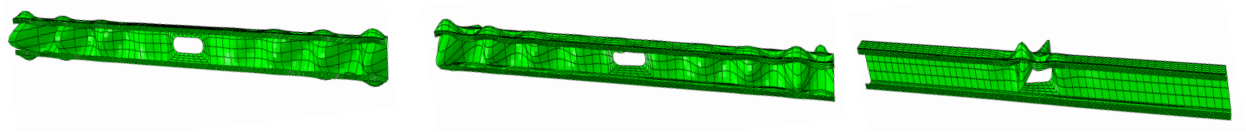

i. ii. iii.

b)

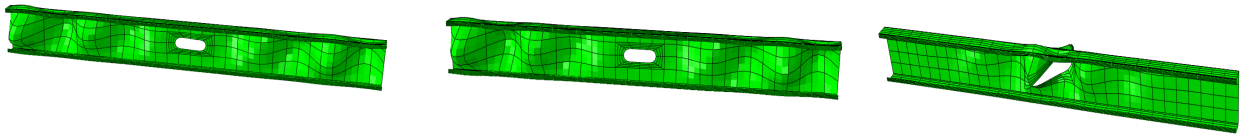

i. ii. iii.

c)

Figure 4: Local buckling modes a) 250S162-33 L24" b) 362S137-33 L48" c) 600S162-33 L48": i) θ=11.31° ii) θ=45° iii) θ=78.69°

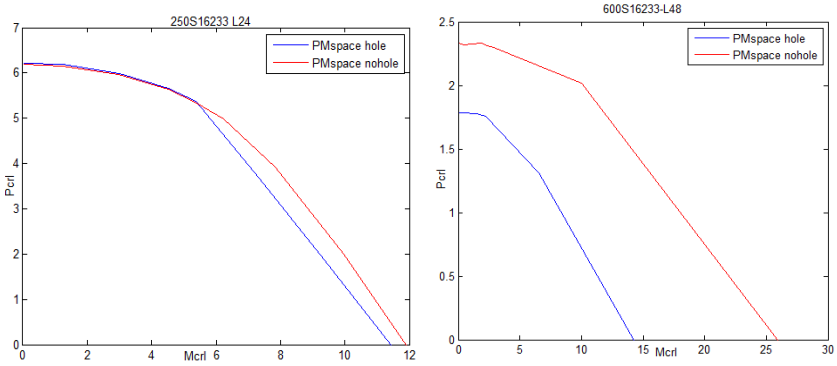

a) b)

Figure 5: Local buckling comparisons for perforated and non-perforated section under combined loading a) 250S162-33 b) 600S162-33

2.3 Distortional stability

The presence of perforations in the web introduces distortional buckling in the flange around the hole as shown in Fig. 6 for SSMA sections 250S162-33, 362S137-33 and 600S162-33, where the unstiffened strips around the hole buckle first triggering the flange to buckle in the same direction because of web-flange interaction. The effect of perforations under combined loading in reducing the distortional buckling magnitudes is shown in Fig. 7.

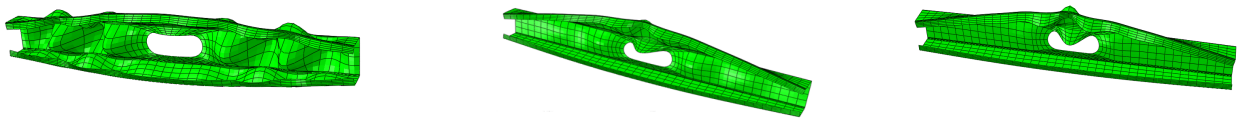

i. ii. iii.

a)

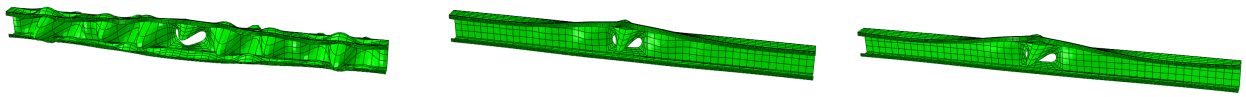

i. ii. iii.

b)

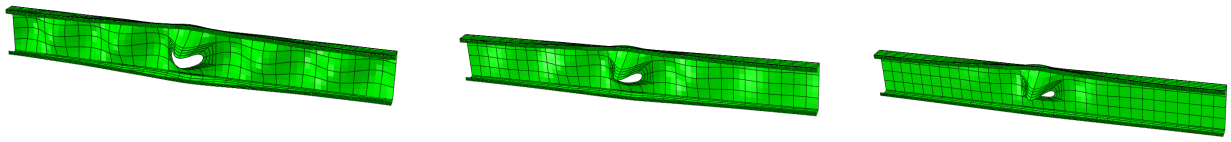

i. ii. iii.

c)

Figure 6: Distortional buckling modes a) 250S162-33 L24" b) 362S137-33 L48" c) 600S162-33 L48": i) θ=11.31° ii) θ=45° iii) θ=78.69°

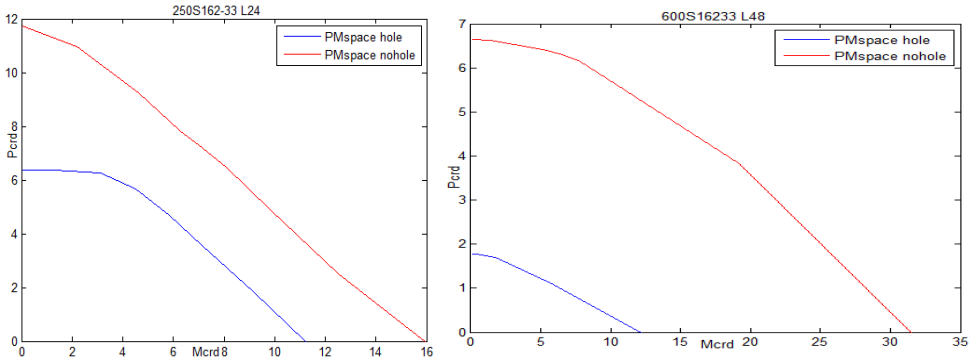

a) b)

Figure 7: Distortional buckling comparisons for perforated and non-perforated section under combined loading a) 250S162-33 b) 600S162-33

2.4 Global stability

SSMA sections were selected to evaluate the global behavior in the P-M space. The parameters varied include length, thickness, number of holes, web height (h) and flange (b) dimensions (250S137-54, L=26in, h=2.5in., b=1.375in., t= 0.0566in.; 400S162-68, L=54in., h=4in., b=1.625in., t=0.0713in.; and 600S250-97, L=92in. h=6in., b=2.5in., t= 0.1017 in.). Hole spacing of 13 in. was varied according to length; short sections having one central hole while longer sections having two or three holes evenly spaced throughout the length. Fig. 8 compares perforated and non-perforated global buckling modes of the SSMA sections, which show no observable deformation effect at the perforations. Section 600S250-97 with the larger thickness of 0.1017 in. resulted in minimal variation in global buckling load between holes and no holes, with the shorter sections showing increased difference between holes and no holes, in particular for the angle θ varying between 0º-80º.

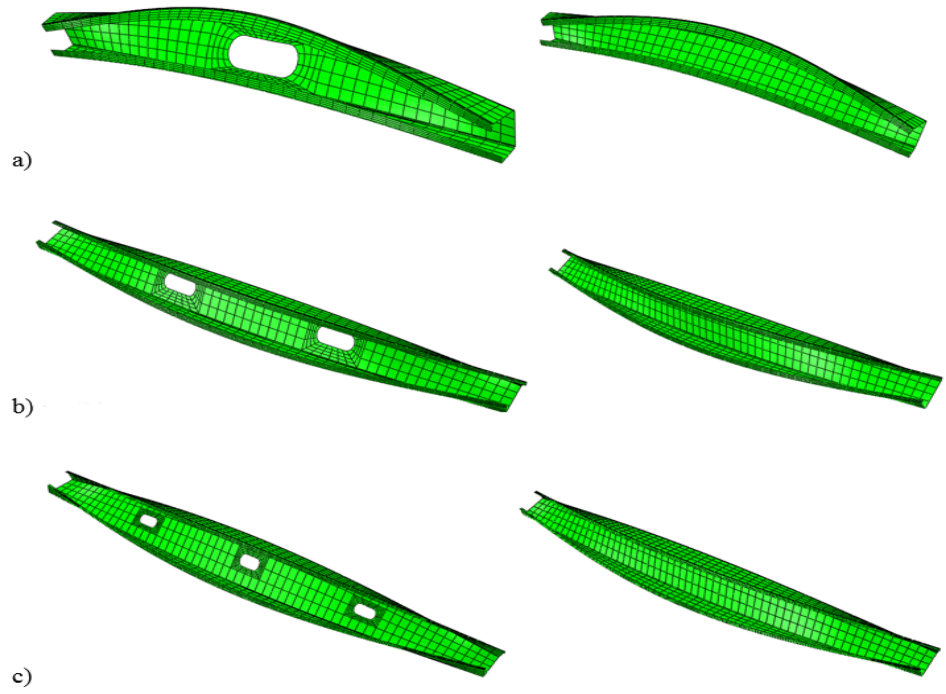

Figure 8: Global buckling modes for perforated and non-perforated sections at θ=45° a) 250S137-54 L26" b) 400S162-68 L54" c) 600S250-97 L92"

3. Collapse analysis of perforated members under combined loading

FE collapse analysis for perforated members subjected to combined loading is carried out using ABAQUS (2013). Non-linear collapse sensitivity to modeling assumptions is examined and benchmark studies are done at existing anchor points for pure loading by comparing the collapse analysis models to experimental studies that were done by Moen (2009).

3.1 Finite element modeling assumptions

Research by Schafer and Pekoz (1998) has provided distribution and magnitudes used in modeling geometric imperfections. Imperfection amplitude-to-thickness ratios (d/t) are provided as a function of cumulative distribution function (CDF) probabilities. In this paper, the initial imperfections are created by superposing the lowest local, distortional and global buckling mode shapes from eigen-buckling analyses. The local and distortional amplitude magnitudes are based on 25% CDF (local: 0.14t, distortional: 0.64t, global: L/2000) and 75% CDF (local: 0.66t, distortional: 1.55t, global: L/1000.)

Cold-formed steel members are created by cold-rolling thin sheet metal, which can generate residual stresses, and plastic strains that in-turn affect the ultimate strength of the member. Moen et.al. (2008) have provided methods of prediction of residual stresses and plastic strains. In this research, however, residual stresses are ignored consistent with previous studies on non-perforated CFS beam-column members done by the authors (Shifferaw (2010)). Material modeling follows von Mises yield criteria, with isotropic hardening (yield stress, fy= 58.6 ksi, E=29500 ksi and Poisson ratio=0.3). The solution type adopted is the

Riks method with initial arc length of 0.25, maximum step size of 0.75 and maximum solution increment of 300.

3.2 Verification study

Existing experimental results for perforations are used in benchmarking. Sections are selected for comparison with the experimental research done by Moen (2011). Fig. 9 shows the cross-sections examined in global studies that include: 400S162-68 (54in), 600S250-97 (92in) and 250S137-54 (26in); and those in distortional studies that include: 600S250-97 (24in), 600S137-68 (24in) and 800S250-97 (24in). Tables 1 and 2 provide the results obtained from the benchmark study in which in both distortion (e.g., avg. 0.96 and std. dev. 0.07) and global cases (e.g., avg. 0.99 and std. dev. 0.07) the FE model predictions agree well with the tests.

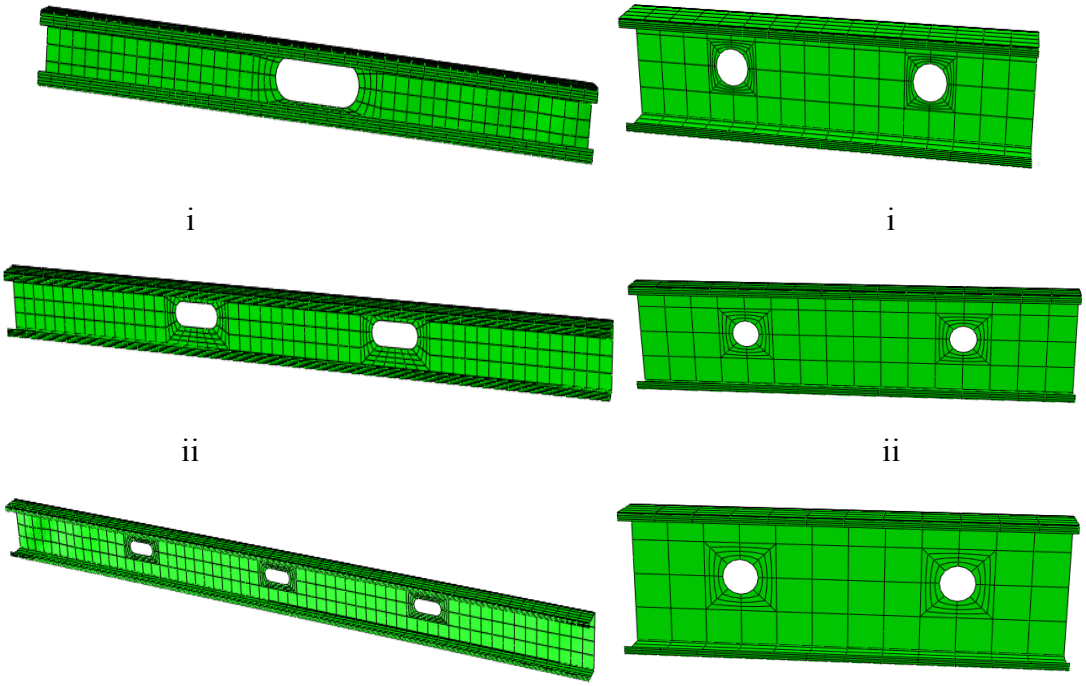

Figure 9: a) Global study sections i) 250S137-54 ii) 400S162-68 iii) 600S250-97 b) distortional study sections i) 600S250-97 ii) 600S137-68 iii) 800S250-97

Table 1: Distortional benchmark results

Section	P_y (k)	P_{crd} (k)	$P^1_{25\%cdf}$(k)	$P^2_{25\%cdf}$(k)	P_{test}/P	$P^1_{75\%cdf}$(k)	$P^2_{75\%cdf}$(k)	P_{test}/P
600S250-97	64.54	51.24	41.9	43.83	.9559	36.2	41.36	.8752
600S137-68	37.22	14.84	18.87	18.09	1.043	17.49	16.38	1.067
800S250-97	74.71	34.15	41.4	46.0	.9	38.1	39.5	.9645
[1]test model [2]benchmark model					Avg=.96 Std. dev=.072			Avg=.96 Std. dev=.096

Table 2: Global benchmark results

Section	L(in)	P^1_{cre}(k)	P^2_{cre}(k)	$P^1_{25\%cdf}$(k)	$P^2_{25\%cdf}$(k)	P_{test}/P	$P^1_{75\%cdf}$(k)	$P^2_{75\%cdf}$(k)	P_{test}/P
400S162-68	54	16.3	15.78	13.66	13.19	1.035	12.36	12.004	1.029
600S250-97	92	25.4	25.60	23.8	23.15	1.028	22.7	20.5	1.107
250S137-54	26	20.8	17.8	9.24	10.21	.9049	8.84	8.65	1.021
[1]test model [2]benchmark model						Avg=.99 Std. dev=.07			Avg=1.05 Std. dev=.04

3.3 Collapse analysis example

Collapse analysis for a 250S162-33 Channel section of length 15 in. with a single centered hole is illustrated in Fig. 10 for θ=0°, θ=45° and θ=90° exhibiting distortional failure mode. For sections with low distortional slenderness, collapse is initiated at the unstiffened strip and the net yield strength at the hole cross section governs. Transitional limits are used to determine whether distortional slenderness lies on the net yield capacity region or the region controlled by elastic buckling. These limits will be defined in the next section.

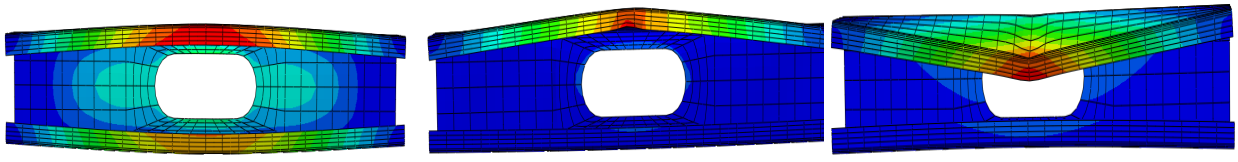

a) b) c)

Figure 10: Collapse mechanism with displacement contours a) θ=0° b) θ=45° c) θ=90°

4. Preliminary Direct Strength Method of perforated members under combined loading

4.1 Global preliminary DSM

The proposed DSM formulation for non-perforated beam-columns by Torabian and Schafer (2014) is modified to consider the influence of holes (with resultant critical buckling load for perforated cross-sections). SSMA section 400S162-68 of length 54 inches with two slotted holes equally spaced is examined where the preliminary DSM prediction is illustrated against the existing linear DSM assumption in Fig. 11. The nominal global capacity, $\boldsymbol{\beta_{nG}}$, is given as:

$$\beta_{nG} = \beta_{nGP} + (\beta_{nGM} - \beta_{nGP})sin\theta \quad (3)$$

Compression; $0 \leq \theta < \pi/2$

$$\beta_{nGP} = 0.658^{\lambda_G{}^2}\beta_y \quad \text{for } \lambda_G \leq 1.5 \quad (4)$$

$$\beta_{nGP} = 0.877\beta_{crG} \quad \text{for } \lambda_G \geq 1.5 \quad (5)$$

Bending; $0 \leq \theta < \pi/2$

$$\beta_{nGM} = \beta_y \quad \text{(no inelastic reserve)} \quad \text{for } \lambda_G \leq 0.60 \quad (6)$$

$$\beta_{nGM} = \frac{10}{9}\beta_y\left(1 - \frac{10\beta_y}{36\beta_{crG}}\right) \quad \text{for } 0.6 < \lambda_G \leq 1.34 \quad (7)$$

$$\beta_{nGM} = \beta_{crG} \quad \text{for } \lambda_G > 1.34 \quad (8)$$

Where

β_{nGP} = Nominal capacity in axial compression

λ_G = Global slenderness

$$\lambda_G = \sqrt{\beta_y / \beta_{crG}} \quad (9)$$

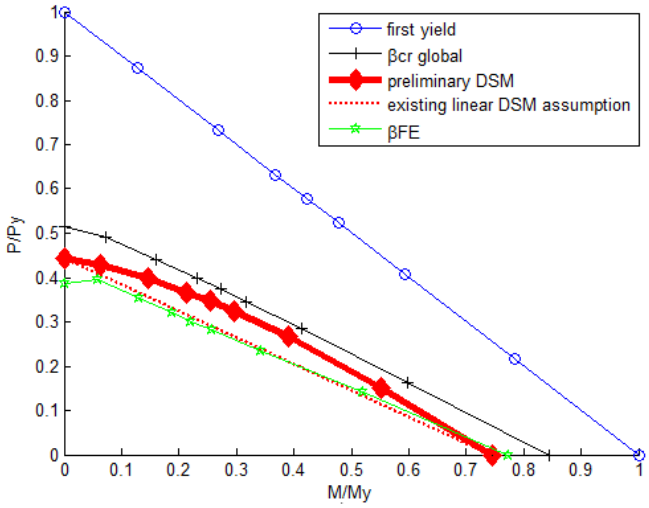

Figure 11: Global preliminary DSM formulation for perforated members

4.2 Local preliminary DSM

Local preliminary DSM equations are presented in Eq.'s (10-18) and are formulated to reduce to the current AISI-S100 2012 equations for perforated beams and columns. When critical load β_{cr} is low relative to yield β_y, elastic buckling controls the column behavior. When slenderness is low, inelastic buckling is initiated at the unstiffened strips, and the capacity goes to inelastic reserve or first yield, if inelastic reserve is ignored. For Section 350S162-54 of length 24 inches with observed local-global interaction, Fig. 12 shows that the local preliminary DSM formulations predict increased capacity approaching yielding near pure bending.

The local slenderness (λ_L) is defined as:

$$\lambda_L = \sqrt{\frac{\beta_{nG}}{\beta_{crL}}} \text{ for } \beta_{nG} \leq \beta_y \quad (10)$$

$$\lambda_L = \sqrt{\frac{\beta_y}{\beta_{crL}}} \text{ for } \beta_{nG} > \beta_y \quad (11)$$

for $\lambda_L \leq 0.776$

Ignoring inelastic reserve capacity:

$$\beta_{nL} = \beta_y \text{ , } \beta_{nG} > \beta_y \quad (12)$$

$$\beta_{nL} = \beta_{nG} \text{ , } \beta_{nG} \leq \beta_y \quad (13)$$

β_{nL} determined should be less than β_{ynet}, the yield at the net cross section area around holes.

$$P_{ynet} = A_{net}\left(\frac{P_y}{A_g}\right) \text{ (net yield at hole due to axial load)} \quad (14)$$

$$M_{ynet} = S_{fnet}\left(\frac{M_y c}{I_{xx}}\right) \text{ (net yield at hole due to bending load)} \quad (15)$$

$$\beta_{ynet} = \sqrt{\left(\frac{P_{ynet}}{P_y}\right)^2 + \left(\frac{M_{ynet}}{M_y}\right)^2} \text{ (normalized net yield at hole due to combined loading)} \quad (16)$$

Where

S_{fnet}= net section modulus referenced to the extreme fiber in first yield

A_{net} = net cross section area at hole

A_g = gross cross section area

c = distance from extreme fiber to center of gravity

I_{xx} = moment of inertia

for $\lambda_L > 0.776$

$$\beta_{nL} = \left[1 - 0.15\left(\frac{\beta_{crL}}{\beta_{nG}}\right)^{0.4}\right]\left(\frac{\beta_{crL}}{\beta_{nG}}\right)^{0.4}\beta_{nG} \qquad \text{for } \beta_{nG} \leq \beta_y \tag{17}$$

$$\beta_{nL} = \left[1 - 0.15\left(\frac{\beta_{crL}}{\beta_y}\right)^{0.4}\right]\left(\frac{\beta_{crL}}{\beta_y}\right)^{0.4}\beta_y \qquad \text{for } \beta_{nG} \geq \beta_y \tag{18}$$

$$\beta_{nL} \leq \beta_{ynet}$$

Where

β_{nL} = nominal local capacity

β_{crL} = critical elastic local buckling load

β_{nG} = is determined in section 4.1

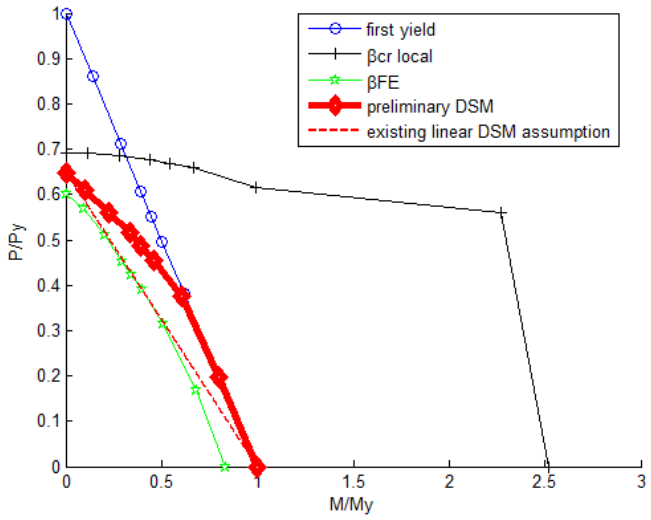

Figure 12: Local preliminary DSM formulation for perforated members

4.3 Distortional preliminary DSM

DSM preliminary formulations provided below (Eq. (19-27)) are modifications of non-perforated study by Torabian and Schafer (2014) and the AISI-S100-12 (2012). For low slenderness failure is initiated by yielding at the hole. When failure is initiated at the hole, the net area A_{net} and net section modulus S_{fnet} at the hole are used in determining the net axial and bending loads respectively. The transitional limits are provided for pure bending and axial loads (AISI-S100 (2012)). Transitional limits that cover the change from failure at the hole to distortional failure are modified to account for location in the P-M space. Preliminary distortional DSM implementation for section 250S162-33 of length 15in. is illustrated in Fig. 13. Distortional-global interaction is ignored similar to DSM in AISI-S100-12 and the nominal capacity is a function of distortional slenderness as follows:

for $\lambda_d \leq \lambda_{d1}$

$$\beta_{nd} = \beta_{ynet} \tag{19}$$

for $\lambda_{d1} < \lambda_d \leq \lambda_{d2}$

$$\beta_{nd} = \beta_{ynet} - \left[\left[\frac{\beta_{ynet}-\beta_{d2}}{\lambda_{d2}-\lambda_{d1}}\right]\langle\lambda_d - \lambda_{d1} sin\theta\rangle\right] \tag{20}$$

for $\lambda_d > \lambda_{d2}$

$$\beta_{nd} = \left[1 - \langle 0.25 - 0.03 sin\theta\rangle \left[\frac{\beta_{crd}}{\beta_y}\right]^{\langle 0.6-0.1 sin\theta\rangle}\right]\left[\frac{\beta_{crd}}{\beta_y}\right]^{\langle 0.6-0.1 sin\theta\rangle} \beta_y \tag{21}$$

Where

$$\lambda_d = \sqrt{\frac{\beta_y}{\beta_{crd}}} \tag{22}$$

$$\lambda_{d1} = \langle 0.561 + 0.112 sin\theta\rangle \left[\frac{\beta_{ynet}}{\beta_y}\right]^{\langle 1+2 sin\theta\rangle} \tag{23}$$

$$\lambda_{d2} = \langle 0.561 + 0.112 sin\theta\rangle \left[\langle 14 - 12.3 sin\theta\rangle \left[\frac{\beta_{ynet}}{\beta_y}\right]^{\langle -0.4+3.1 sin\theta\rangle} - \langle 13 - 12.3 sin\theta\rangle\right] \tag{24}$$

$$\beta_{d2} = \sqrt{P_{d2}^2 + M_{d2}^2} \tag{25}$$

$$P_{d2} = (1 - \left(1 - 0.5{\lambda_{d2}}^{-1.2}\right)^2) P_y \tag{26}$$

$$M_{d2} = (1 - 0.22\left(\frac{1}{\lambda_{d2}}\right))(\frac{1}{\lambda_{d2}}) M_y \tag{27}$$

λ_{d1} = the limit beyond which capacity is given by the net yield strength

λ_{d2} = transitional limit of distortional slenderness

β_{ynet}= defined in the section 4.2

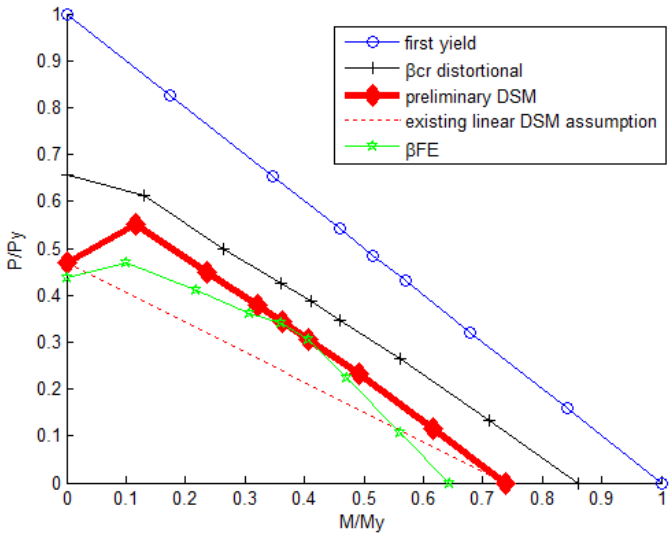

Figure 13: Distortional preliminary DSM formulation for perforated members

5. Conclusions

Stability of perforated cold-formed steel members, common in the framing industry, subjected to combined loading has been examined. Elastic buckling and yielding envelopes that form the basis of the Direct Strength Method are established for selected SSMA sections. Localized buckling deformation effect triggered by the unstiffened strips around the holes under different resultant loads are observed. The presence of perforations reduces the elastic critical buckling resultant load (in local, distortional and global modes) in comparison with non-perforated members. Preliminary Direct Strength Method for local, distortional and global limit states in perforated members under combined actions have been formulated considering yielding and elastic critical buckling envelopes in the P-M space for the influence of holes. Results indicate that stability and yielding of perforated cold-formed steel beam-columns under the appropriate stress combinations need to be considered rather than simply making the linear interaction assumption that does not accurately reflect the collapse behavior. Combined with future work on examining behavior of perforated members under generalized bending (minor and major axes including inelastic reserve) for non-symmetric sections, these results provide valuable analytical background in future experimental testing to develop final Direct Strength Method provisions for combined loading of perforated cold-formed steel members.

References

1. Schafer, B.W. (2006). "Direct Strength Method design guide." *American Iron and Steel Institute*, Washington DC.
2. AISI-S100. (2012). *North American Specification for the design of cold-formed steel structural members, Washington, D.C.*.
3. Shifferaw, Y., Schafer, B.W. (2010). "Towards a direct strength method for cold-formed steel beam-columns." *Annual Stability Conference*, Orlando, Florida: Structural Stability Research Council. 613-630.
4. Yared Shifferaw. (2010). "Section capacity of cold-formed steel members by the direct strength method." *Ph.D. Thesis*, Johns Hopkins University, Baltimore.
5. Schafer, B.W., Z. Li, and C.D. Moen. (2010). "Computational modeling of cold-formed steel*." Thin-Walled Structures*, 48(10-11) 752-762.
6. Moen, C.D. (2009). "Direct strength design of cold-formed steel members with perforations*." Ph.D. Thesis*, Johns Hopkins University, Baltimore.
7. ABAQUS. (2013). "ABAQUS/Standard Version 6.13-1*."* Dassault-Systems, Editor, Providence,RI.
8. Schafer B.W., Pekoz.T. (1998). "Computational modelling of cold-formed steel: characterizing geometric imperfections and residual stresses." *Journal of Constructional Steel Research*, 47(3)193-210.
9. Moen, C.D., Igusa, T. and Schafer, B.W. (2008). "Prediction of residual stresses and strains in cold-formed steel members." *Thin-Walled Structures*, 46(11) 1274-1289.
10. Moen, C.D., Schafer, B.W. (2011). "Direct strength method for design of cold-formed steel columns with holes*." Journal of Structural Engineering*, 137(5) 559-570.
11. Torabian, B.Z., Schafer, B.W. (2014). "Development of a new beam-column design method for cold-formed steel lipped channel members." *22nd international specialty conference on recent research and development in cold-formed steel design and construction*, St. Louis, Missouri. 359-375.